Title
Catalysis of PAH biodegradation by humic acid shown in synchrotron infrared studies

Journal
Environmental Science and Technology, 36(6)

Authors
Holman, Hoi-Ying N.
Nieman, Karl
Sorensen, Darwin L.
et al.

Publication Date
2001-09-26

Catalysis of PAH Biodegradation by Humic Acid Shown in Synchrotron Infrared Studies

Hoi-Ying N. Holman[1*], Karl Nieman[2], Darwin L. Sorensen[2], Charles D. Miller[3], Michael C. Martin[4], Thomas Borch[5], Wayne R. McKinney[4], Ronald C. Sims[2]

[1]Center for Environmental Biotechnology, Lawrence Berkeley National Laboratory, Berkeley, CA 94720

[2]Utah Water Research Laboratory, Utah State University, Logan, UT 84321

[3]Biology Department, Utah State University, Logan, UT 84321

[4]Advanced Light Source Division, Lawrence Berkeley National Laboratory, Berkeley, CA 94720

[5]Center for Biofilm Engineering, Montana State University, Bozeman, MT 59717

Abstract

The role of humic acid (HA) in the biodegradation of toxic polycyclic aromatic hydrocarbons (PAHs) has been the subject of controversy, particularly in unsaturated environments. By utilizing an infrared spectromicroscope and a very bright, nondestructive synchrotron photon source, we monitored *in situ* and over time the influence of HA on the degradation of pyrene (a model PAH) by a bacterial colony on a magnetite surface. Our results indicate that HA dramatically shortens the onset time for PAH biodegradation from 168 to 2 hours. These results will have large implications for the bioremediation of contaminated soils.

---

* To whom correspondence should be addressed. Email: hyholman@lbl.gov

Introduction

Humic acids (HAs) are complex organic molecules produced by the decomposition of plant and animal remains in soils. The surfactant-like micellar microstructure of HA (*1,2*) is thought to accelerate the degradation of polycyclic aromatic hydrocarbons (PAHs) (*3*) by enhancing PAH solubility (*4,5*), thereby increasing the PAH bioavailability to microorganisms. Despite abundant evidence that HA is important in the bioremediation of several anthropogenic pollutants (*6-8*), its role in the detoxification of PAHs by microbes remains uncertain.

Reports of the effects of HA on the biodegradation of PAHs in aqueous and water-saturated geological environments are contradictory, some showing increased degradation (*9-12*), some inhibition (*11,13,14*), and others no effect (*15*). Few studies have evaluated HA effects in unsaturated geological environments (such as the vadose zone), where research tools are generally limited to analysis of extracted contaminants (*16*) or the use of radio-labeled tracers to follow contaminant fate among humic acid, fulvic acid, and humin fractions (*17*). The results of these studies were also inconclusive. However, the addition of humic-rich compost in unsaturated geological systems has been shown to increase biological degradation of PAH more than amendment with either fertilizer or bacteria (*16,18,19*).

These inconclusive results motivate a novel approach to the study of this important biogeochemical process. To determine the effects of HA on the bioremediation of PAH

with confidence requires a nondestructive microprobe with chemical specificity, one that can track and identify the progress of PAH biotransformation, with and without HA, in a single bacterium or colony of bacteria on a mineral surface. Synchrotron radiation-based Fourier transform infrared (SR-FTIR) spectromicroscopy is such a tool. With a signal-to-noise ratio far superior to that of conventional FTIR systems (*20*), SR-FTIR spectromicroscopy yields unique infrared signatures for each of the components of the biotransformation system at spatial resolutions smaller than 10 microns, the size of a small colony of bacteria.

We used SR-FTIR spectromicroscopy to examine the effects of soil HA on biodegradation of the model PAH pyrene in the presence of a colony of *Mycobacterium sp.* JLS, on a mineral surface in an unsaturated environment. Infrared spectra measured during the onset and progress of biodegradation constitute the first microscopic study of this process to be made in real time.

Procedure

SR-FTIR spectra were obtained from samples of *M. sp.* JLS as they degraded pyrene on magnetite surfaces, with and without the addition of Elliott Soil Humic Acid (ESHA). The ESHA used in this study was the International Humic Substances Society's humic acid standard, well-characterized and chemically very stable, which is prepared from Elliott soil, typical of the prairie soils of the United States. ESHA improves aeration and water-holding capacity and provides a more hospitable environment for microorganisms, but it is a poor source of energy for their growth and development

(*21*). The pyrene-degrading microorganism *M. sp.* JLS is a gram-positive, rod-shape bacterium (GenBank accession no. AF387804); our samples were recently isolated from PAH-contaminated soil at the Libby Groundwater Superfund Site in Libby, Montana, USA. Our mineral substrates were freshly cleaved surfaces of small chips (less than 1 cm in diameter) of magnetite rock from Minerals Unlimited of Ridgecrest, CA; magnetite is a ubiquitous component of geologic materials (*22*) and is efficient in the adsorption of bacteria cells (*23*).

The chips were cleaned by sonication in deionized and organic-free water and sterilized by ultraviolet irradiation. A thin film of pyrene was placed on most magnetite surfaces by using 1 - 5 μl of 1000-ppm pyrene (spectroscopy grade; Sigma) dissolved in hexane (spectroscopy grade; Sigma). The hexane was allowed to evaporate, forming a thin film of pyrene, and IR spectroscopy verified that the pyrene-coated magnetite surfaces were free of residual hexane. The surfaces of magnetite chips used as pyrene-free controls were prepared in a similar manner but with pure hexane. For some magnetite chips, an additional 1 μl of an aqueous solution of 300-ppm filter-sterilized ESHA at pH 7 was applied on top of the pyrene film. Other magnetite chips received 1 μl of plain deionized, organic-free water at pH 7. All the resultant samples were incubated in a humidified, 30ºC air incubator for four weeks to allow them to equilibrate.

We began the time-dependent pyrene biodegradation experiment by adding 2.5 μl of cell suspension (~1.5×10^8 cells/milliliter) of *M. sp.* JLS onto the prepared magnetite chips. A custom IR microscope-stage mini-incubator was used to maintain the proper

growth conditions for *M. sp.* JLS, while allowing *in situ* FTIR spectromicroscopy measurements. For abiotic controls, no *M. sp.* JLS was applied.

SR-FTIR spectromicroscopy measurements were performed at Beamline 1.4.3 of the Advanced Light Source at Lawrence Berkeley National Laboratory, Berkeley, CA, USA, using a Nicolet Magna 760 FTIR bench and Nic-Plan IR microscope. The synchrotron infrared light is focused to a diffraction-limited spot size of 3 - 10 ìm diameter on a computer-controlled x-y-z sample stage, and the beam is fiducially located within the field of the microscope to approximately one micron, using a titanium pattern on a silicon calibration target. We have recently demonstrated that the intense synchrotron infrared beam has no effect on living biological systems (*24, 25*).

Infrared spectra were acquired in the standard reflectance mode from selected portions of the samples, those areas flat enough to be within the depth of focus of the IR microscope and which showed the appropriate compounds in the IR spectra. The same locations on each sample were revisited to obtain a time series of spectra, with the frequency of sampling and the optimum schedule of revisiting based on results from two sets of exploratory experiments. All SR-FTIR spectra were recorded in the 4000-650 cm^{-1} region, as this mid-IR region contains unique molecular absorption fingerprints for all molecules of interest in our study. Every IR measurement consisted of 128 co-added spectra at a spectral resolution of 4 cm^{-1}, ratioed to a reference spectrum similarly collected from a gold-coated glass slide. Any residual water-vapor features remaining in the resultant spectrum were removed by subtracting an appropriately scaled water-

vapor spectrum. ESHA, pyrene, and *M.* sp. JLS each have distinct absorption bands which we used as chemical markers to elucidate the role of ESHA in the dynamics of pyrene degradation. Non-overlapping spectral markers were selected to monitor each component.

Results

Figure 1 summarizes the time series of infrared spectra obtained by repeatedly measuring the same location on each pyrene-coated sample for more than a month. Panels (a) and (c) show details of the IR spectra centered on the C-H bending mode of pyrene at 1185 cm^{-1}, and in panels (b) and (d) the pyrene C-H stretching doublet at 3044 and 3027 cm^{-1} is shown plus peaks from the biomass methyl groups at 2921 and 2850 cm^{-1} (*26*). Panels (a) and (b) show spectra from samples without ESHA, while spectra in panels (c) and (d) are from samples containing ESHA. Insets to all panels show spectra from the corresponding abiotic samples. Since the sample surface is different for each experimental condition, the absolute value of the absorbance between different samples can vary. However by monitoring the same position on each sample individually, the changes in absorption peaks in presented in each panel are quantitative. Over a similar period, the infrared spectra obtained from samples free of pyrene did not show statistically significant changes.

For surfaces with living *M. sp.* JLS, the intensities of the 1185, 3044 and 3027 cm^{-1} pyrene peaks decrease systematically over time, corresponding to a reduction in the amount of pyrene present at the measurement location. As the biodegradation process

proceeded, there were drastic changes in IR absorption intensities. Compare the insets for each panel of Fig. 1, which show that abiotic systems, whether or not ESHA was added, exhibited only minor changes in pyrene absorption peaks as a function of time.

For samples without ESHA, pyrene biodegradation starts very slowly, and about 168 hours elapse before significant changes are observed. Biodegradation then proceeds quickly, and all the observed pyrene is completely degraded within the next 35 hours. As the pyrene peaks in the spectra disappear, we observe an increase in the biomass IR absorption peaks, implying concurrent biomass formation during the consumption of pyrene (Fig. 1, panels (a) and (b)). By contrast, the biodegradation of pyrene on samples with ESHA begins almost immediately (~1 hour) after the introduction of *M. sp.* JLS (Fig. 1, panels (c) and (d)). The degradation of the observed pyrene is complete by the fourth hour. Again we detect an increase in biomass absorption during the later stage of the pyrene degradation, which implies that biomass formation is concurrent with the consumption of pyrene. The presence of ESHA significantly shortens the time of pyrene degradation by *M. sp.* JLS.

To better understand the long 168-hour onset time for samples without ESHA, in Figure 2 we compare the initial IR spectrum with one acquired near the onset of pyrene degradation. An increase in absorbance between 1100 and 1130 cm^{-1} is clearly seen and is associated with the C O stretching of glycolipids. In contrast, no similar increase in glycolipids is observed during the onset of PAH biodegradation when ESHA is present (not shown). Apparently the HA solubilizes the PAH, making it immediately

available for bacterial uptake. The long onset time may therefore be interpreted as the time required for *M. sp.* JLS to produce a sufficient amount of extracellular, surfactant-like biomolecules, such as glycolipids, which solubilize pyrene and thereby make it available for bacterial uptake.

Figure 3 displays pyrene concentration and biomass versus time under three different conditions, as measured by associated spectral absorbances normalized to remove surface effects as described above. Abiotic results show that pyrene remains on the mineral surface, with only slow removal mechanisms. One of these is probably sorption at the intra-particle level caused by diffusion into pores of the magnetite. Evaporation and sublimation may also play a minor role. Pyrene degradation by *M. sp.* JLS without ESHA did not proceed until ~ 170 hours after the introduction of the bacteria, followed by a rapid decrease of pyrene and a rapid increase of biomass within the next thirty-five hours, as described earlier. After the pyrene was depleted the biomass signal significantly decreased, presumably as the *M. sp.* JLS bacteria transformed themselves into ultramicrocells, a starvation-survival strategy commonly observed among bacteria in oligotrophic environments (*21*). In the presence of ESHA, pyrene biodegradation begins within an hour and the observed pyrene is depleted by the end of the fourth hour, with a concurrent increase of biomass. Both the degradation of pyrene and the increase of biomass corroborate the effectiveness of ESHA in radically accelerating biodegradation of pyrene. It is likely that the water-insoluble pyrene is solubilized into the cores of ESHA pseudo-micelles and therefore becomes directly available for bacterial uptake and consumption, as suggested by Engebretson *et al.* (*1*).

Over longer times, IR absorption bands of pyrene on magnetite surfaces showed a slight increase and decrease. The increase is probably due to pyrene diffusing from pyrene trapped in micropores (≤ 0.5 μm in diameters) of the magnetite and/or neighboring surfaces of higher pyrene concentration. Our method of introducing pyrene onto the sample surfaces and the subsequent four-week sample equilibration inside a humidified incubator allows pyrene to enter magnetite micropores too small for bacteria to reside. Thus (by analogy to the work of Bosma *et al.* (*27*)), the first wave of rapid depletion of pyrene by *M. sp.* JLS set up a diffusion gradient from the pyrene-containing micropores toward the bacterial colony, leading to a subsequent small increase in pyrene concentration. For the surface containing ESHA, the biomass remained almost constant over a period of more than 200 hours, indicating that the flux of pyrene from the micropores was sufficient to maintain the bacterial colony. Results reported by Wick et al. (*28*) corroborate mass transfer of PAH and its concurrent biodegradation. For the surface free of ESHA, there is little evidence of the presence of a quasi-steady state biomass. To clarify this phenomenon longer monitoring will be needed.

At the end of the time-resolved experiment (t ~ 460 hours), spatial distributions of pyrene, *M. sp*. JLS, and ESHA were measured by acquiring infrared spectra every 5 microns across the center of the bacterial colony with ESHA (the sample described in Fig. 1, panels (c) and (d)). Figure 4 shows contour maps of the spatial distribution of measured infrared absorbances corresponding to *M. sp*. JLS, ESHA, and pyrene. The middle of the maps is an area with a high population density of *M. sp*. JLS and a high

concentration of ESHA. At the beginning of the experiment, this central region showed a high concentration of pyrene (the basis for selecting this particular region for study). At the end of the experiment, pyrene in this region was completely biodegraded. Where pyrene is present without *M. sp*. JLS, there is no significant degradation.

Discussion

Our results have significant implications for the bioremediation of contaminated soils. In many PAH-contaminated sites, such as the Libby Superfund site located in Libby, Montana, USA (*29*), bioremediation is specified by the U.S. Environmental Protection Agency as the preferred remedial technology. Bioremediation of PAH-contaminated soils is often limited, however, by the low solubility of PAH, which inhibits microbial uptake (*30*). Adding synthetic surfactants to enhance PAH solubility (*31,32*) may be toxic to natural microorganisms and further inhibit bioremediation (*31,33*). Based on results reported here, a potential alternative in unsaturated soil environments may be the application of natural HA to accelerate the biodegradation of PAH.

SR-FTIR spectromicroscopy can assess real-time interactions between multiple constituents in contaminated soils. Combined with conventional mineralization measurements, which monitor respiration through carbon dioxide production, SR-FTIR spectromicroscopy is a powerful tool for evaluating bioremediation options and designing bioremediation strategies for contaminated vadose zone environments.

Acknowledgements

For their comments on this paper we thank Prof. A.B. Cunningham and Prof. J.W. Costerton of the Center for Biofilm Engineering at Montana State University, Dr. T.C. Hazen of the Center of Environmental Biotechnology, and Ms. M. Kauffman of the Department of Biological Sciences and Department of Geology, Idaho State University. We also thank Paul Preuss and Art Robinson for critical readings of the manuscript. The Advanced Light Source is supported by the Director, Office of Science, Office of Basic Energy Sciences, Materials Sciences Division, of the U.S. Department of Energy under Contract No. DE-AC03-76SF00098 at Lawrence Berkeley National Laboratory.

References

1. Engebretson, R. R.; Von Wandruszka, R. *Environmental Science & Technology* **1994**, *28*, 1934-1941.

2. Chiou, C. T.; Kile, D. E.; Brinton, T. I.; Malcolm, R. L.; Leenheer, J. A.; Maccarthy, P. *Environmental Science & Technology* **1987**, *21*, 1231-1234.

3. Autho In *In Situ and On-Site Bioremediation Symposium*; Alleman, B. C., Leeson, A., Eds.; Battelle Press: New Orleans, 1997; Vol. 2, pp 185-190.

4. Kopinke, F.-D.; Georgi, A.; Mackenzie, K. *Environmental Science & Technology* **2001**, *35*, 2536-2542.

5. Tiehm, A.; Stieber, M.; Werner, P.; Frimmel, F. H. *Environmental Science & Technology* **1997**, *31*, 2570-2576.

6. Haluska, L. U.; Barancikova, G.; Balaz, S.; Dercova, K.; Vrana, B.; Paz-Weisshaar, M.; Furciova, E.; Bielek, P. *Science of the Total Environment* **1995**, *175*, 275-285.

7. Barkovskii, A. L.; Adriaens, P. *Environmental Toxicology and Chemistry* **1998**, *17*, 1013-1020.

8. Fu, Q. S.; Barkovskii, A. L.; Adriaens, P. *Environmental Science & Technology* **1999**, *33*, 3837-3842.

9. Tranvik, L. J.; Hoefle, M. G. *Applied and Environmental Microbiology* **1987**, *53*, 482-488.

10. Larsson, P.; Okla, L.; Tranvik, L. J. *Applied and Environmental Microbiology* **1988**, *54*, 1864-1867.

11. Seibel, F.; Heidenreich, S.; Frimmel, F. H. *Acta Hydrochimica et Hydrobiologica* **1996**, *24*, 260-266.

12. Ortega-Calvo, J.-J.; Saiz-Jimenez, C. *Applied and Environmental Microbiology* **1998**, *64*, 3123-3126.

13. Shimp, R.; Pfaender, F. K. *Applied and Environmental Microbiology* **1985**, *49*, 402-407.

14. Burgos, W. D.; Pisutpaisal, N.; Tuntoolavest, M.; Chorover, J.; Unz, R. F. *Environmental Engineering Science* **2000**, *17*, 343-351.

15. Amador, J. A.; Alexander, M. *Soil Biology and Biochemistry* **1988**, *20*, 185-192.

16. Kaestner, M.; Mahro, B. *Applied Microbiology and Biotechnology* **1996**, *44*, 668-675.

17. Nieman, J. K. C.; Sims, R. C.; Sims, J. L.; Sorensen, D. L.; McLean, J. E.; Rice, J. A. *Environmental Science & Technology* **1999**, *33*, 776-781.

18. Sims, J. L.; Sims, R. C.; Matthews, J. E. *Hazardous Waste & Hazardous Materials* **1990**, *7*, 117-150.

19. Autho In *Bioremediation of chlorinated and polycyclic aromatic hydrocarbons*; Hinchee, R. E., Leeson, A., Semprini, L., S.K., O., Eds.; Lewis: Boca Raton, FL, 1994; pp 203-217.

20. Holman, H.-Y. N.; Perry, D. L.; Martin, M. C.; Lamble, G. M.; McKinney, W. R.; Hunter-Cevera, J. C. *Geomicrobiology J.* **1999**, *16*, 307-324.

21. Morita, R. Y. *Bacteria in oligotrophic environments: starvation-survival lifestyle*; Chapman & Hall: New York, 1997.

22. Kostka, J. E.; Nealson, K. H. *Abstracts of the General Meeting of the American Society for Microbiology* **1995**, *95*, 343.

23. Wong, P. K.; Fung, K. Y. *Enzyme and Microbial Technology* **1997**, *20*, 116-121.

24. Martin, M. C.; Tsvetkova, N. M.; Crowe, J. H.; McKinney, W. R. *Appl Spectrosc* **2001**, *55*, 111-113.

25. Holman, H.-Y. N.; Bjornstad, K. A.; McNamara, M. P.; Martin, M. C.; McKinney, W. R.; Blakely, E. A. *Journal of Biomedical Optics* **2001**, *Submitted*.

26. Smith, B. *Infrared Spectral Interpretation: A Systematic Approach*; CRC: New York, 1999.

27. Bosma, T. N. P.; Middeldorp, P. J. M.; Schraa, G.; Zehnder, A. J. B. *Environmental Science & Technology* **1997**, *31*, 248-252.

28. Wick, L. Y.; Colangelo, T.; Harms, H. *Environmental Science & Technology* **2001**, *35*, 354-361.

29. Sims, R. C.; Sims, J. L.; Sorensen, D. L.; McLean, J. E. "Champion International Superfund Site, Libby, Montana: Bioremediation Field Performance Evaluation of the Prepared Bed Land Treatment System," National Risk Management Research Laboratory, U.S. Environmental Protection Agency, 1996.

30. Smith, J. R.; Egbe, M. E.; Lyman, W. J. In *Bioremediation of Contaminated Soils*; Adrinao, D. C., Bollag, J.-M., Frankenberger, J., W.T., Sims, R. C., Eds.; American Society of Agronomy, Inc.: Madison, WI, USA, 1999; pp 665-717.

31. Laha, S.; Luthy, R. G. *Environmental Science & Technology* **1991**, *25*, 1920-1930.

32. Grimberg, S. J.; Stringfellow, W. T.; Aitken, M. D. *Applied and Environmental Microbiology* **1996**, *62*, 2387-2392.

33. Edgehill, R. U. In *Bioremediation of Contaminated Soils*; Adrinao, D. C., Bollag, J.-M., Frankenberger, J., W.T. , Sims, R. C., Eds.; American Society of Agronomy, Inc.: Madison, WI, USA, 1999; pp 665-717.

Figure Captions

Figure 1. Time series of SR-FTIR absorption bands corresponding to pyrene and biomass formation following the degradation of pyrene by *Mycobacterium* sp. JLS on magnetite surfaces. Panels (a) and (b) are spectra from a sample without ESHA; panels (c) and (d) are from a sample with ESHA. The time at which each spectrum was acquired is labeled. Panels (a) and (c) are centered on a pyrene absorption band at 1185 cm^{-1}. Panels (b) and (d) show a pyrene doublet at 3044 and 3027 cm^{-1} and biomass IR absorption bands at 2921 and 2850 cm^{-1}. Inserts are time series from abiotic control experiments.

Figure 2. Comparison of SR-FTIR spectra at the beginning of the experiment and at the onset of pyrene degradation on the sample without ESHA. Lower panel shows the difference between these two absorbance spectra. An increase in absorbance between 1100 and 1130 cm^{-1} is clearly observed and is associated with the C O stretching of glycolipids produced by the bacteria to solubilize the pyrene.

Figure 3. Summary of IR results showing that pyrene degradation occurs much faster when ESHA is present (note the log scale on the time axis). The color scheme is black for abiotic, green for biotic without ESHA, and red for biotic with ESHA. The solid lines show the pyrene amount as a function of time for each experiment. The dotted lines show a subsequent increase in *Mycobacterium* sp. JLS biomass after pyrene degradation.

Figure 4. Contour diagrams from infrared mapping obtained at the end of the experiment showing the spatial distribution of the infrared absorption peaks corresponding to (top) *Mycobacterium* sp. JLS bacteria, (middle) ESHA, and (bottom) pyrene. Appropriate spectral regions were integrated for each point on the maps. The color scales for each contour plot are red for high integrated IR peak area (high concentration of the corresponding component) and blue for low peak area (low concentration); black is an out of focus region of the sample. The center of the map shows a region with high density of bacteria and high concentration of ESHA, where pyrene has been completely degraded.

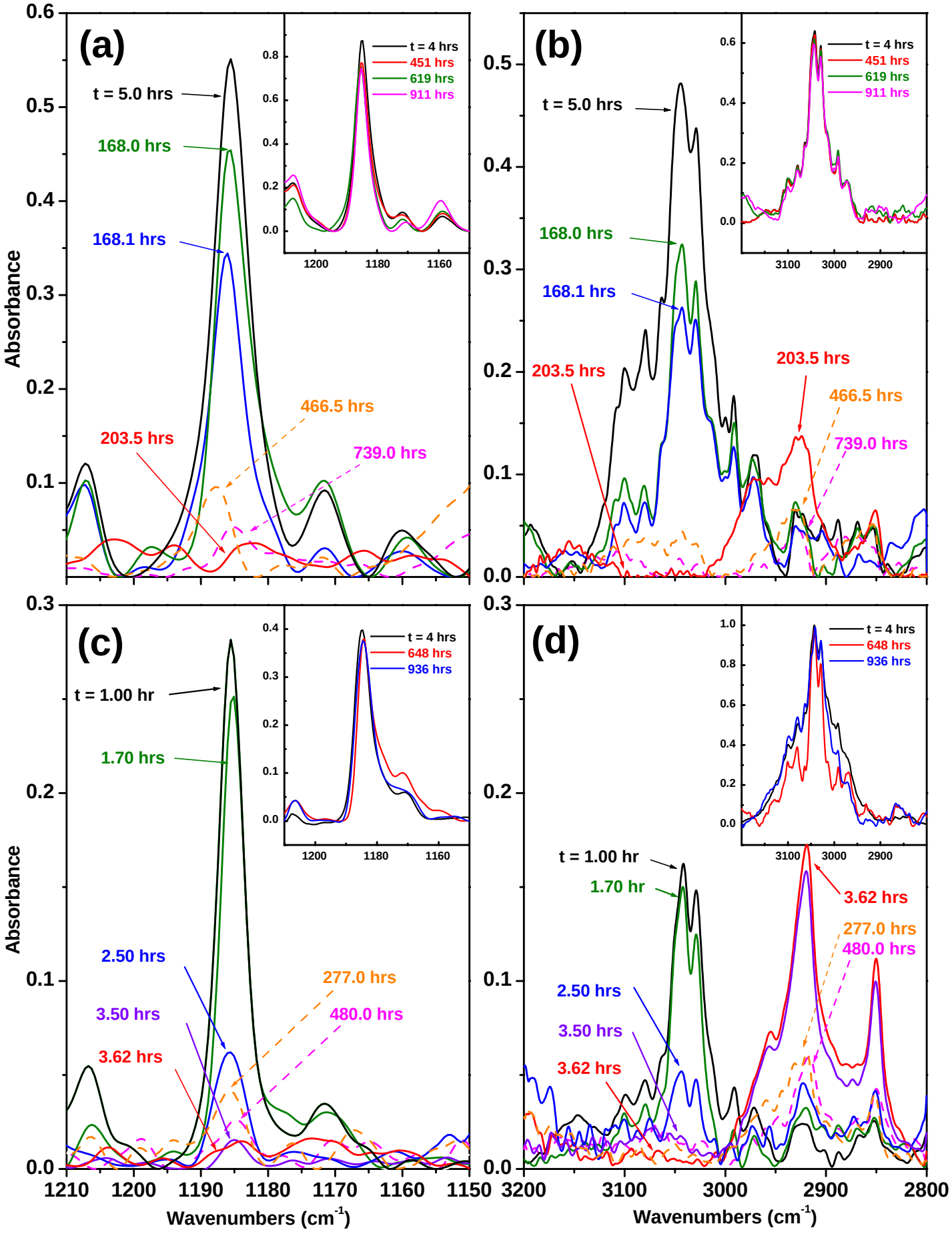
(a)
t = 5.0 hrs
168.0 hrs
168.1 hrs
203.5 hrs
466.5 hrs
739.0 hrs
t = 4 hrs
451 hrs
619 hrs
911 hrs
(b)
t = 5.0 hrs
168.0 hrs
168.1 hrs
203.5 hrs
203.5 hrs
466.5 hrs
739.0 hrs
t = 4 hrs
451 hrs
619 hrs
911 hrs
(c)
t = 1.00 hr
1.70 hrs
2.50 hrs
3.50 hrs
3.62 hrs
277.0 hrs
480.0 hrs
t = 4 hrs
648 hrs
936 hrs
(d)
t = 1.00 hr
1.70 hr
3.62 hrs
277.0 hrs
480.0 hrs
2.50 hrs
3.50 hrs
3.62 hrs
t = 4 hrs
648 hrs
936 hrs
Absorbance
Absorbance
Wavenumbers (cm-1)
Wavenumbers (cm-1)

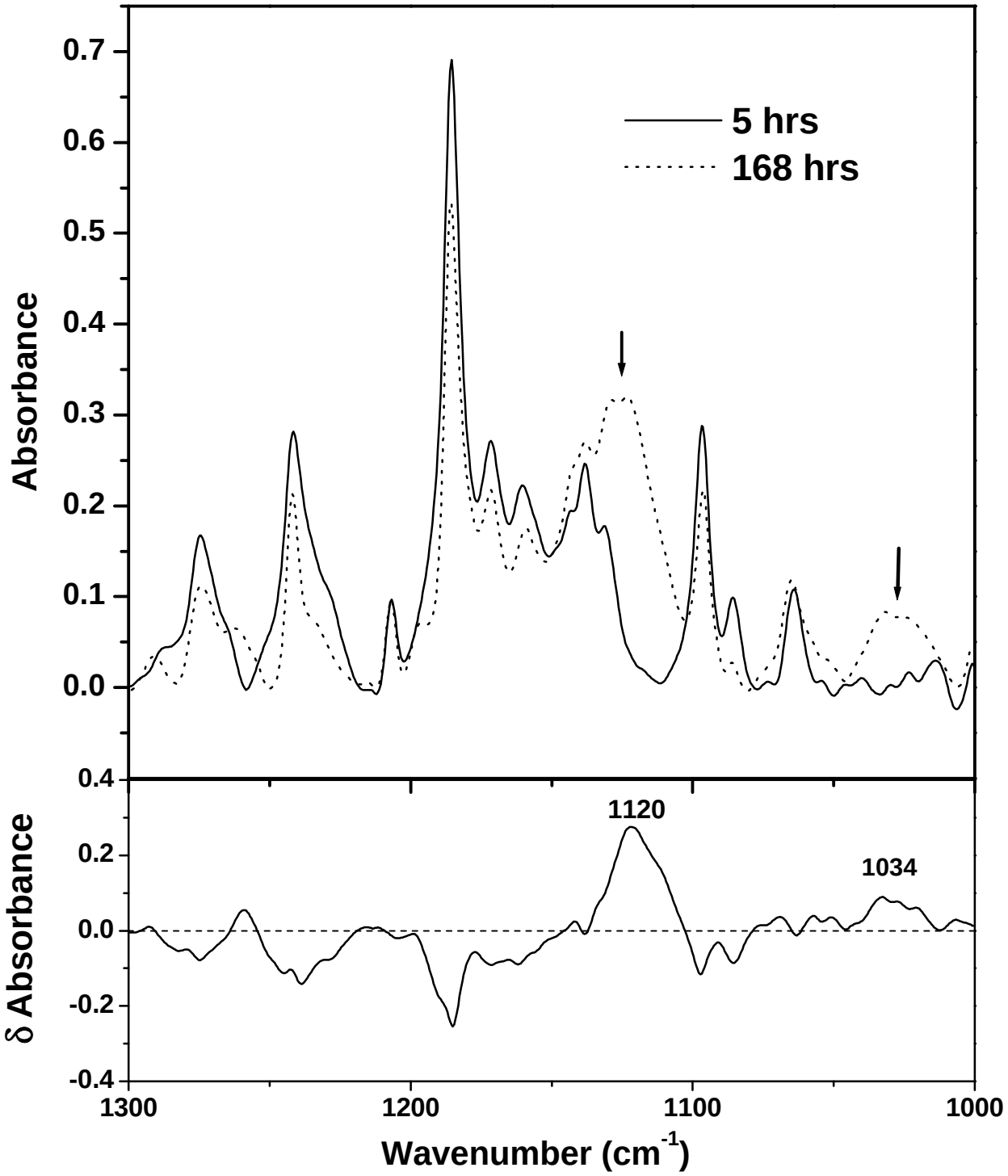
5 hrs
168 hrs
Absorbance
0.7
0.6
0.5
0.4
0.3
0.2
0.1
0.0
0.4
δ Absorbance
1120
1034
0.2
0.0
-0.2
-0.4
1300
1200
1100
1000
Wavenumber (cm-1)

Fig. 2

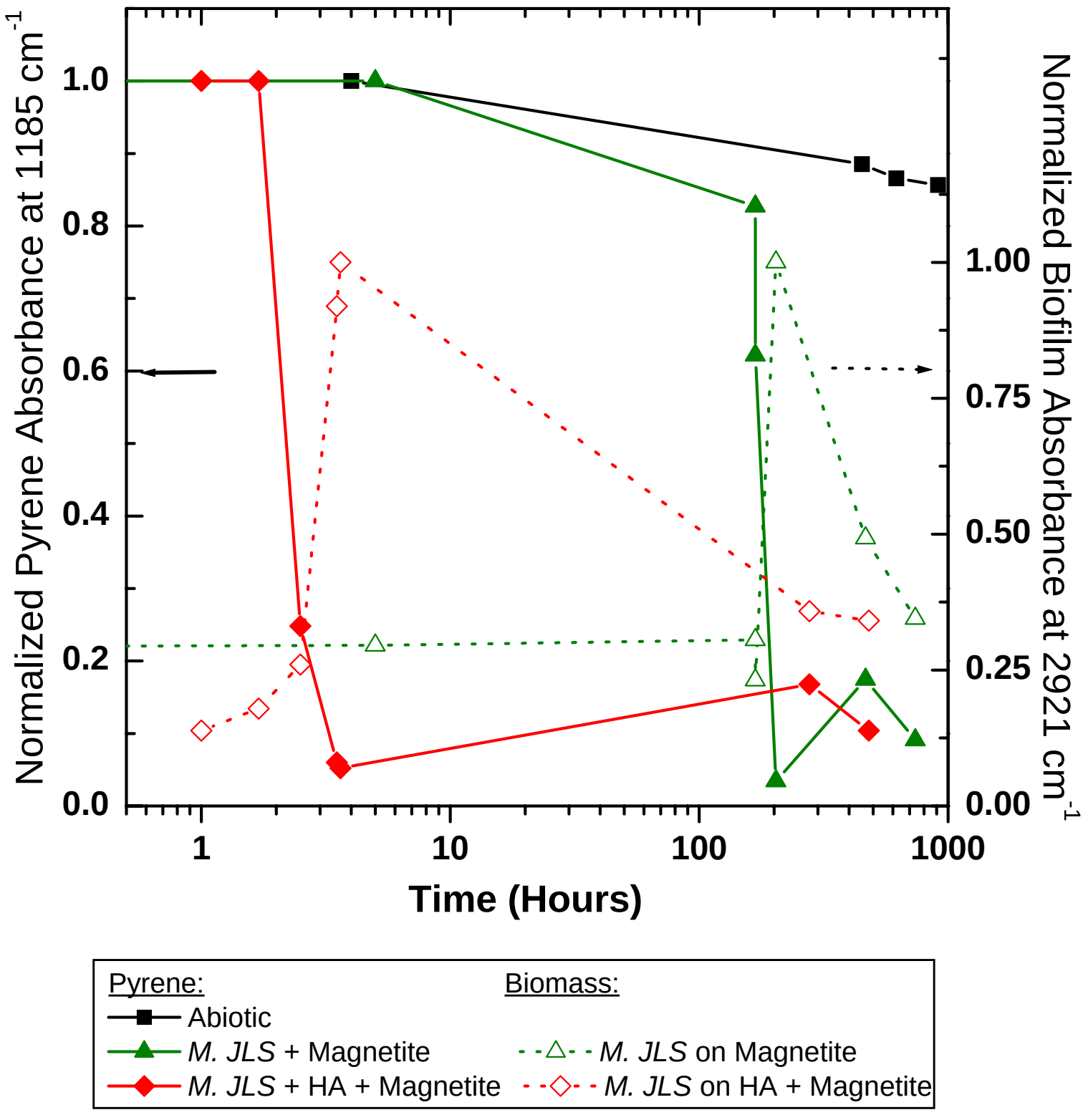
Normalized Pyrene Absorbance at 1185 cm-1
Normalized Biofilm Absorbance at 2921 cm-1
Time (Hours)
1.0
0.8
0.6
0.4
0.2
0.0
1.00
0.75
0.50
0.25
0.00
1
10
100
1000
Pyrene:
Biomass:
Abiotic
M. JLS + Magnetite
M. JLS + HA + Magnetite
M. JLS on Magnetite
M. JLS on HA + Magnetite

Fig. 3

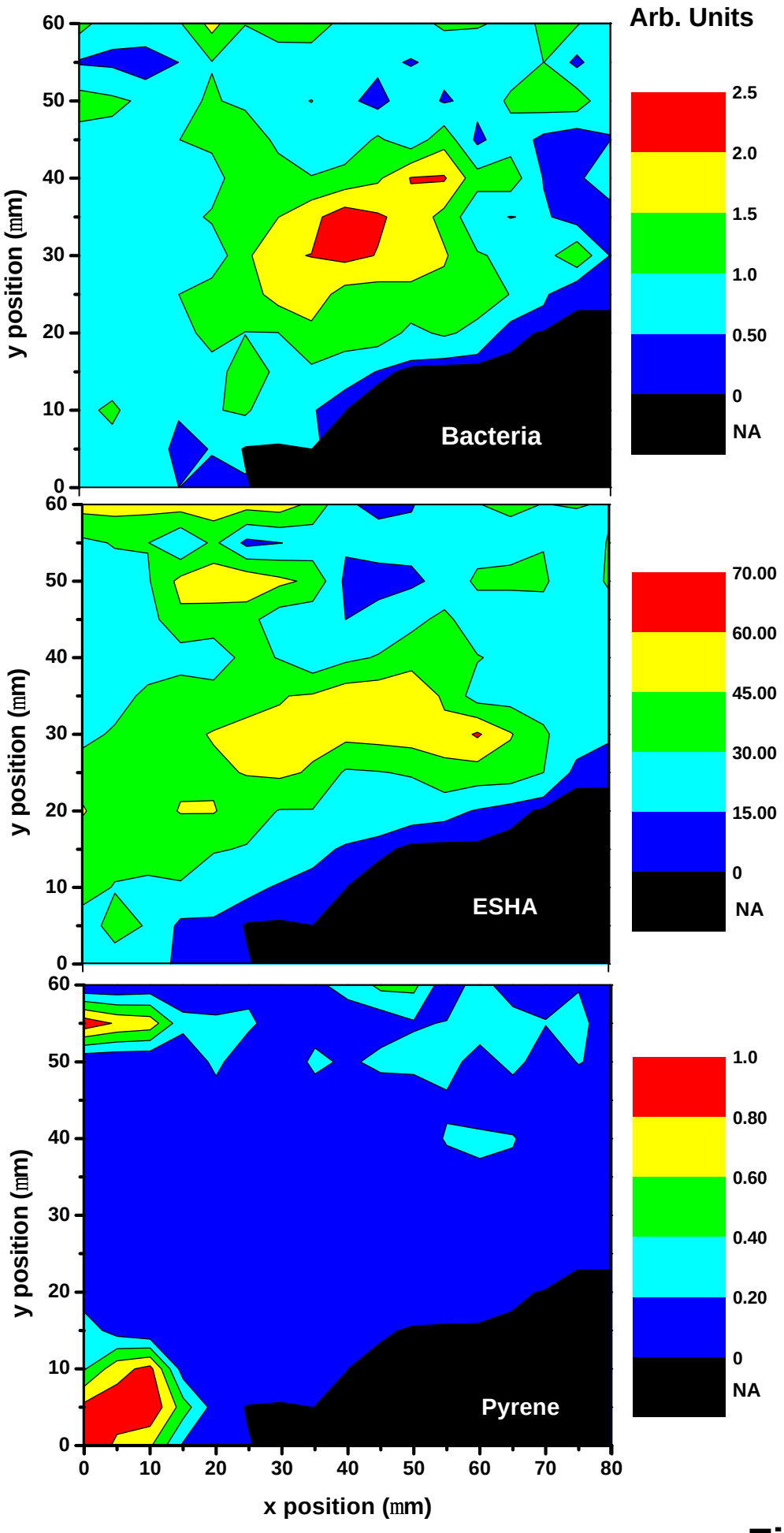
Arb. Units
2.5
2.0
1.5
1.0
0.50
0
NA
Bacteria
y position (mm)
70.00
60.00
45.00
30.00
15.00
0
NA
ESHA
1.0
0.80
0.60
0.40
0.20
0
NA
Pyrene
0 10 20 30 40 50 60 70 80
x position (mm)

Fig. 4